


Tunable magnetic interactions in mono-transition metal spinels MgCr_2X_4 ($X = \text{O}, \text{S}, \text{Se}$) and ACr_2S_4 ($A = \text{Ca}, \text{Sr}, \text{Ba}$)

Zhao Ran,¹ Chengyang Xu,¹ and Weidong Luo^{1,2,*}

¹Key Laboratory of Artificial Structures and Quantum Control (Ministry of Education), School of Physics and Astronomy, Shanghai Jiao Tong University, Shanghai 200240, China

²Institute of Natural Sciences, Shanghai Jiao Tong University, Shanghai 200240, China

 (Received 25 February 2022; revised 21 January 2023; accepted 2 February 2023; published 23 February 2023)

We investigate the electronic and magnetic properties of the spinel materials MgCr_2X_4 ($X = \text{O}, \text{S}, \text{Se}$) and ACr_2S_4 ($A = \text{Ca}, \text{Sr}, \text{Ba}$), a special type of mono-transition metal spinel material. The magnetic properties of these materials are understood by inspecting the competition between the 90° ferromagnetic superexchange interactions and the antiferromagnetic direct exchange interactions. We found the direct exchange interaction is extremely sensitive to the distance between the Cr ions, $d_{\text{Cr-Cr}}$. The overall magnetic interaction can be transformed from antiferromagnetic at short $d_{\text{Cr-Cr}}$ to ferromagnetic at larger $d_{\text{Cr-Cr}}$. Therefore, we can realize different magnetic states in the same material by controlling the $d_{\text{Cr-Cr}}$ with external strain. Furthermore, the ferromagnetism is strengthened as tensile strain is employed, and a strategy to improve the Curie temperature, which is essential for spintronics devices, is proposed.

DOI: [10.1103/PhysRevMaterials.7.024417](https://doi.org/10.1103/PhysRevMaterials.7.024417)

I. INTRODUCTION

Ferromagnetic semiconducting materials that integrate the functionalities of semiconducting and ferromagnetic (FM) properties play important roles in spintronics, modern transistor applications of ultrahigh-density integrated circuits, and magnetic random access memories [1–4]. Unfortunately, the low transition temperature T_c of ferromagnetic semiconductors limits their applications in spintronic devices. The previously reported common ferromagnetic semiconductors, including EuO (77 K) [5], CdCr_2S_4 (90 K) [6], and SeCuO_3 (25 K) [7], have low transition temperatures. Their T_c are close to room temperature for only a few ferromagnetic and semiconducting double perovskite materials, such as $\text{La}_2\text{NiMnO}_6$ (280 K) [8], and the recently reported Sr_3OsO_6 [9] films have an evaluated T_c of about 1060 K. But the ferromagnetic state at such a high temperature is unexpected and counterintuitive, which has not been fully understood [10].

In the present work, we propose that strain engineering (we consider hydrostatic strain, which maintains the cubic symmetry of the original crystal) can be used to improve T_c of the mono-transition metal (MTM) spinel semiconducting and ferromagnetic materials by studying the dependence of magnetic coupling on the strain. The spinel structure can provide versatile compounds to realize a variety of functionalities for device applications. In the normal spinel structure AB_2O_4 , the A^{2+} ions are tetrahedrally coordinated (A site), while the B^{3+} ions are octahedrally coordinated (B site) by oxygen ions. In some spinel compounds, however, partial A^{2+} ions exchange with the B^{3+} ions to form inverse spinel structures. In CoFe_2O_4 [11,12], the Co^{2+} ions occupy the B sites, with half of the Fe^{3+} ions occupying the A sites and the

other half occupying the B sites. In partial inversion spinel structures, the ratio of the A and B site interchange can range from 0 to 1, resulting in spinel compounds possessing various properties. In addition, the cations in A sites and B sites can be both transition metal and non-transition metal elements. In CoFe_2O_4 [11,12], both A sites and B sites are occupied with transition metal elements. However, in MgAl_2O_4 [13], the A sites and B sites are both non-transition metal elements. The magnetic and electronic properties in double transition metal elements spinel materials are complicated because of multiple exchange interactions involved [14–22]. In the present work, we focus on only the AM_2X_4 type spinel materials, where A is +2 nonmagnetic cations, M is +3 magnetic cations, and X is chalcogenide anions. Since M is the only transition metal element in AM_2X_4 , we call it a MTM spinel material, such as SiFe_2O_4 , SiCo_2O_4 , and SiNi_2O_4 .

Here we study one type of MTM spinel material, the thiospinels, as an example [23–25]. Our study shows that they are tunable semiconducting and ferromagnetic materials. The magnetic state in these compounds is determined by the competition between the direct exchange interaction J_{dd} and the 90° superexchange interaction J_{dpd} . When J_{dpd} dominates all exchange interactions, the materials will manifest ferromagnetic features. On the other hand, the classical frustrated antiferromagnetic (AFM) states will emerge. J_{dd} and J_{dpd} are closely related to the hopping between the orbitals, and their strength is determined by the distance $d_{M_1-M_2}$ of the two metal ions. As $d_{M_1-M_2}$ can be manipulated with external strain, the magnetic states in MTM spinel materials can be controlled correspondingly by the strain method. Furthermore, the ferromagnetic properties can be enhanced under appropriate strain.

The thiospinels possess a variety of magnetic characters depending on the type of anions. MgCr_2O_4 is AFM with a reported Néel temperature in the range of 15–20 K [26–28]. MgCr_2S_4 is FM according to first-principles calculations.

*wdluo@sjtu.edu.cn

Although it has been synthesized by different methods [24,25], its magnetic and electronic properties have not been explored in detail. Here we also study the isoelectronic compound MgCr_2Se_4 , which is formed by substituting the S atoms in MgCr_2S_4 with the larger Se atoms and was predicted to be thermodynamically stable [29]. Furthermore, by substituting the Mg atoms in MgCr_2S_4 with the larger Ca, Sr, or Ba atoms, we obtain the new isoelectronic compounds (Ca, Sr, Ba) Cr_2S_4 . Our first-principles calculations show that, compared to MgCr_2S_4 , the magnetic exchange couplings in these new compounds are also enhanced. Based on experimental observations and our theoretical calculations, we conjecture that the magnetic states in the MTM spinel materials can be tuned by external strain instead of only by substituting the anions. There is a critical point where materials are transformed from AFM states to FM states. As a consequence, we can implement both FM and AFM states in the same material by controlling only the strain strength.

II. METHODS

First-principles density functional theory (DFT) [30,31] simulations were performed based on the plane-wave basis, as implemented in the Vienna Ab initio Simulation Package (VASP) [32,33]. The projector augmented wave [34,35] potentials were used, and the wave functions were expanded on the plane-wave basis with a kinetic energy cutoff of 500 eV. In most of the calculations, the exchange-correlation energy functional was described by the generalized gradient approximation (GGA) with the Perdew-Burke-Ernzerhof scheme [36]. The Brillouin zone integration was sampled by a $4 \times 4 \times 4$ k -point mesh for structure relaxation, an $8 \times 8 \times 8$ mesh for self-consistent electronic calculation, and a $10 \times 10 \times 10$ mesh for the density of states (DOS) calculation [37]. To relax the original structure, the positions of the ions and the crystal lattice were both relaxed until the Hellman-Feynman forces became less than 10^{-3} eV/Å.

The dynamical stability of MgCr_2S_4 and MgCr_2Se_4 was studied by calculating their phonon spectra, with the help of the PHONOPY package [38] using density functional perturbation theory [39,40]. To test whether our results are robust, the electron correlation effect of the Cr $3d$ electrons in MgCr_2S_4 was also treated with the GGA + U approximation. Here we applied a spherically averaged scheme where only $U_{\text{eff}} = U - J$ is independent [41].

III. STRUCTURAL AND ELECTRONIC PROPERTIES

A. Crystal structure

MgCr_2X_4 ($X = \text{O}, \text{S}, \text{and Se}$) crystallize in the normal spinel structure, with Cr^{3+} ions octahedrally and Mg^{2+} tetrahedrally coordinated by X ions. All three materials are predicted to be dynamically stable by first-principles thermodynamics calculations [29]. The lattice constants in both the experimental and computationally optimized structures are summarized in Table I. The lattice constants predicted by the non-spin-polarized DFT calculation are smaller than the experimental structure. The structure parameters of the compounds (Ca, Sr, Ba) Cr_2S_4 are given in Table I, which shows our idea for the scheme of substituting ions for

TABLE I. The lattice constants a_0 of MgCr_2X_4 ($X = \text{O}, \text{S}, \text{and Se}$) in the experimental and relaxed structures and $d_{\text{Cr-Cr}}$ between the nearest-neighbor (NN) and the next-nearest-neighbor (NNN) Cr ions of the relaxed structure. By A site substitution of MgCr_2S_4 with Ca, Sr, or Ba atoms, the relaxed structures of the three new compounds are also listed.

	a_0 (Å)		$d_{\text{Cr-Cr}}$ (Å)	
	Expt.	DFT relax	NN	NNN
MgCr_2O_4	8.334	8.254	2.918	5.054
MgCr_2S_4	10.143	9.968	3.524	6.104
MgCr_2Se_4		10.535	3.725	6.452
CaCr_2S_4		10.358	3.662	6.342
SrCr_2S_4		10.550	3.729	6.459
BaCr_2S_4		10.726	3.792	6.567

high- T_c FM materials. We also list the nearest-neighbor (NN) and next-nearest-neighbor (NNN) distances $d_{\text{Cr-Cr}}$ in Table I. $d_{\text{Cr-Cr}}$ plays an essential role in the magnetic properties of the thiospinels, which will be shown clearly in the following.

MgCr_2S_4 was synthesized recently with different experimental techniques [24,25]. For the isoelectronic compound MgCr_2Se_4 , however, a valuable synthesis technique is still lacking. We calculated the phonon spectrum of MgCr_2Se_4 , which shows the compound is dynamically stable. It is expected that MgCr_2Se_4 will be synthesized in the future, as it was also predicted to be thermodynamically stable [29].

B. Electronic structure

The electronic band structures were calculated in ferromagnetic configurations for thiospinels. Since the magnetic ground state in the spin of Cr is geometry frustrated [42], the band structures are calculated without spin polarization for MgCr_2O_4 . Figure 1(a) indicates that MgCr_2O_4 is a metal. The local coordinates used in the calculations are shown in Fig. 1(d). MgCr_2X_4 ($X = \text{S}$ and Se) are indirect band gap semiconductors, which agree well with the results calculated with the full-potential linearized augmented plane-wave with local orbitals method [23]. The band gaps are 0.82 and 0.70 eV for MgCr_2S_4 [Figs. 1(b) and 1(e)] and MgCr_2Se_4 [Figs. 1(c) and 1(f)], respectively. The atomic orbital projection of the band structures shows that the t_{2g} orbitals of Cr ions are half occupied, while the e_g orbitals are empty, which agrees with the magnetic moment of $\sim 3 \mu_B$ per Cr ion with Cr^{3+} in the high-spin state. Furthermore, exchange splitting between the t_{2g} majority spin and minority spin is sizeable. As a result, an insulating gap emerges between the majority spin t_{2g} and minority spin e_g orbitals.

IV. MAGNETIC PROPERTIES

A. Heisenberg exchange model

According to our understanding of the electronic structures of thiospinels in Sec. III, the magnetic moment in Cr ions is localized, and the materials are insulating. Hence, we project the exchange interactions between Cr ions in thiospinels to the Heisenberg model, which will make it easy to understand the magnetic states. As indicated by the lattice constants

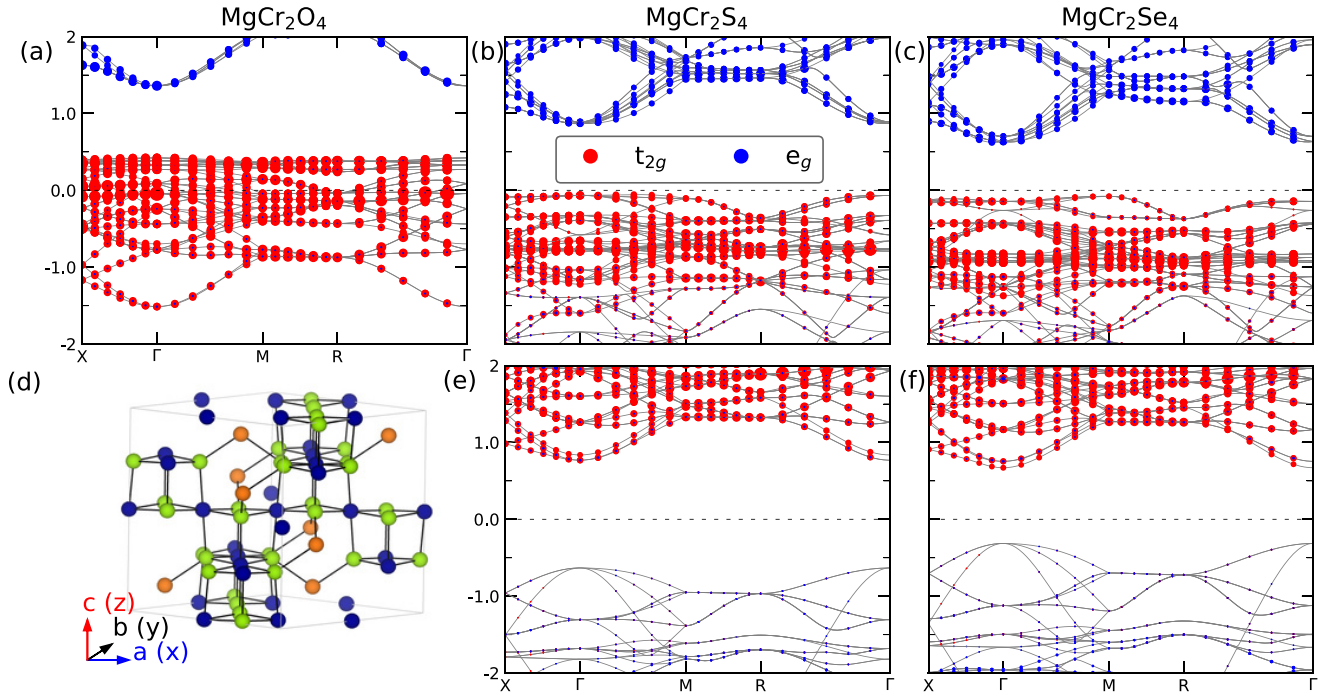


FIG. 1. The energy band structures of (a) MgCr_2O_4 , (b) the majority spin of MgCr_2S_4 , (e) the minority spin of MgCr_2S_4 , (c) the majority spin of MgCr_2Se_4 , and (f) the minority spin of MgCr_2Se_4 . (d) The crystal structure; blue, light green, and brown spheres are B site, anion, and A site atoms. x - y - z and a - b - c are the local and global coordinates, respectively. Here the t_{2g} orbitals of Cr are shown by red solid dots, and the e_g orbitals are represented by blue solid dots; the size of the dots represents the weight of the orbitals in the band wave functions. The valence band maximum is set to zero for clarity.

and the distance between the ions of thiospinels summarized in Table I, the distance of Cr ions with the third NN is substantially longer than the first-NN distance. The long-distance separation between ions implies that the exchange interactions in the third NN are negligible. Therefore, we ignore the exchange interactions beyond the NNN to make the problem tractable, as shown in Fig. 2(d). Under this approximation, the Heisenberg Hamiltonian H is written as

$$H = -\frac{1}{2} \sum_{i,j} J_1 \mathbf{S}_i \cdot \mathbf{S}_j - \frac{1}{2} \sum_{i,l} J_2 \mathbf{S}_i \cdot \mathbf{S}_l, \quad (1)$$

where J_1 and J_2 are the nearest-neighbor and next-nearest-neighbor exchange interactions, respectively. \mathbf{S}_i and \mathbf{S}_j are classical spin vectors, with the magnitude set to $3/2$. We set up three magnetic configurations [as shown in Figs. 2(d)–2(f)] in cubic unit cells to extract these interaction coefficients, which illustrate the magnetic properties of the materials directly. For example, if $J > 0$, FM exchange interactions between the corresponding neighbors are preferable. Otherwise, AFM exchange interactions are preferred.

Based on the three magnetic structure configurations, the Heisenberg Hamiltonian simplifies to the following parameterized forms:

$$E_{\text{FM}} = -108J_1 - 216J_2 + E_0, \quad (2)$$

$$E_{\text{AFM1}} = 18J_1 - 36J_2 + E_0, \quad (3)$$

$$E_{\text{AFM2}} = 18J_1 - 18J_2 + E_0, \quad (4)$$

where J_1 and J_2 can be obtained by solving the three linear equations, in which the total energy for the three magnetic configurations of the cubic unit cell was computed with the DFT method. In the relaxed crystal structure, the three J_1 are -10.92 , 1.01 , and 2.32 meV for MgCr_2X_4 ($X = \text{O}, \text{S}, \text{and Se}$), respectively. The NNN exchange coupling coefficients J_2 are 0.42 meV (MgCr_2O_4), 0.36 meV (MgCr_2S_4), and 1.52 meV (MgCr_2Se_4). It is not a surprise that J_2 are much smaller than J_1 . According to these J_1 and J_2 , we conclude that the MgCr_2O_4 is strongly AFM and the other two are FM. The different magnetic states in MgCr_2X_4 provide us a way to manipulate the magnetic materials by substituting the anion.

The FM and AFM states in thiospinels can be understood based on the direct exchange interaction J_{dd} and 90° superexchange interaction J_{dpd} exchange mechanism in transition metal compounds [43]. The latter is an important part of the Goodenough-Kanamori-Anderson rules [44–46]. As schematically shown in Fig. 2, the exchange interactions in the edge-sharing octahedra of Cr ions in spinel structure include two exchange channels. The first one is J_{dpd} , as shown in Figs. 2(a) and 2(b), in which the exchange interactions between Cr ions are mediated by the anions. The second exchange channel is J_{dd} , as depicted in Fig. 2(c), and originates from the Cr t_{2g} orbitals overlapping directly in the diagonal direction of the Cr square lattice. J_{dd} in the AFM arrangement are more energetically competitive than in the FM alignment. The energy in the AFM order is lowered by about $\Delta E \sim t_{dd}^2/U$ with respect to the FM state (where t_{dd} is the direct hopping parameter between the two t_{2g} orbitals of Cr and U is the Coulomb repulsion energy) [43]. On the

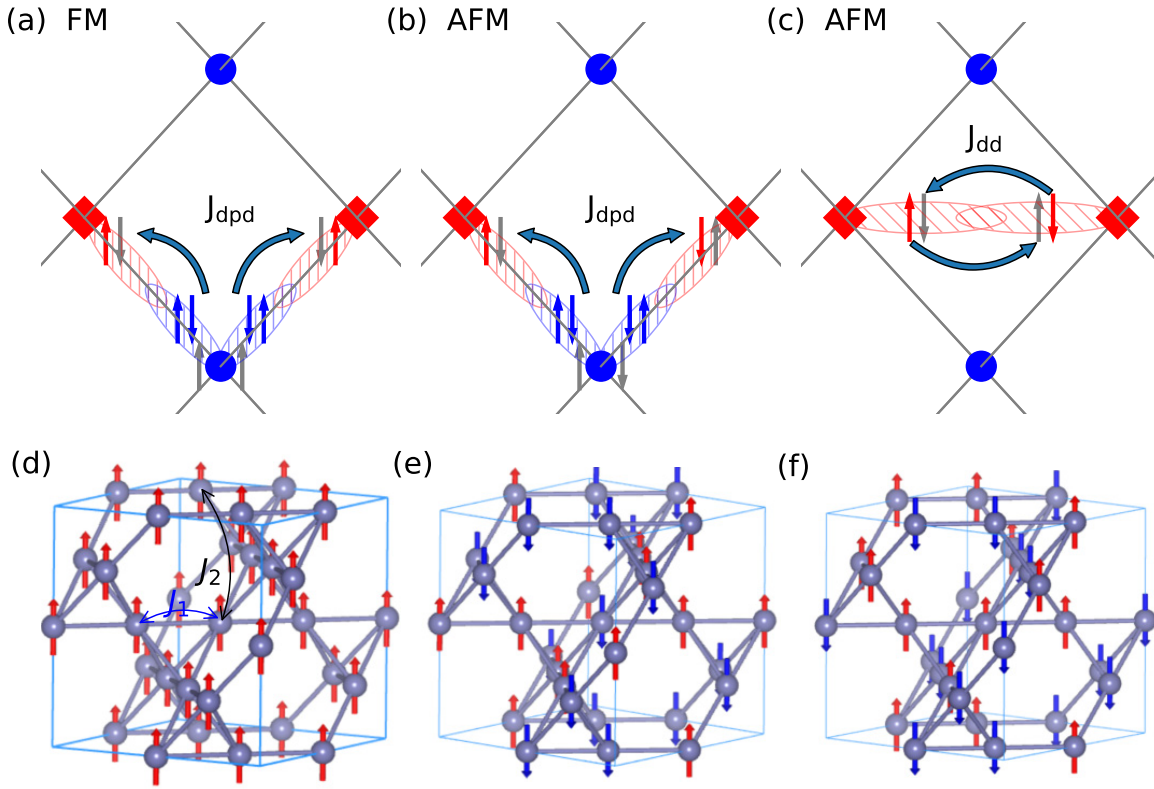


FIG. 2. The exchange interactions and the magnetic configurations in the thiospinels. (a)–(c) are plotted in the x - y plane involving the B sites and the anion sites in the spinel structure. The 90° superexchange interaction J_{dpd} between the nearest-neighbor (NN) Cr ions is shown for (a) the FM and (b) AFM spin configurations; (c) the direct exchange interaction J_{dd} between the NN Cr spins in the AFM configuration. The gray arrows represent the intermediate states after the electron hopping. The Cr ions are represented by red squares, and the anions are shown by blue spheres. Three magnetic configurations, (d) FM, (e) AFM1, and (f) AFM2, are considered to compute the exchange coupling coefficients. J_1 and J_2 are the NN and the next-nearest-neighbor (NNN) exchange interactions, respectively. Only the cations at B sites in cubic spinel are shown for clarity. The blue and red arrows denote spin-up and spin-down sites, respectively.

contrary, J_{dpd} in the FM configuration gains more energy than in the AFM configuration. The FM arrangement is preferred because it satisfies Hund's first rule in the single anion since the parallel arrangement of the remaining electron in anions [the gray arrows in Fig. 2(a)] gains Hund's energy J_H .

The competition between J_{dd} and J_{dpd} is the reason for the complex and diverse magnetic structures in spinel materials. Previous research results show that MgCr_2O_4 is a classical pyrochlore Heisenberg antiferromagnet with frustrated magnetism [26,42,47]. The strong antiferromagnetic state is due to the formidable overlapping of t_{2g} orbitals between the Cr ions. The small radius of the oxygen ions results in a shorter distance between Cr ions. That is, J_{dd} dominates the overall exchange interactions in MgCr_2O_4 . On the other hand, the p - d hybridized bonding becomes stronger from oxygen to sulfur compounds. As a result of the ionic radius being larger in sulfur than oxygen, the distance between the Cr ions in MgCr_2S_4 becomes much longer than that in MgCr_2O_4 ; the NN $d_{\text{Cr-Cr}}$ in MgCr_2O_4 is 0.6 \AA smaller than that in MgCr_2Se_4 , as summarized in Table I. Now, J_{dpd} is the most important exchange interaction in MgCr_2S_4 and MgCr_2Se_4 , giving rise to their FM property.

We conjecture reasonably that MgCr_2S_4 is a FM material because of the long $d_{\text{Cr-Cr}}$. As shown in Table I, $d_{\text{Cr-Cr}}$ in MgCr_2X_4 becomes longer as X varies from O to Se.

Consequently, the transition between AFM and FM orders is intimately related to the type of anions. Looking into the structure of the two different magnetic materials, we envisage the direct overlap of t_{2g} orbitals between the Cr ions becomes weak in MgCr_2S_4 and MgCr_2Se_4 . Inspired by the transition of the magnetic state, in the following we propose a scheme that controls the magnetic properties in MTM spinel materials through external hydrostatic strain engineering which is directly related to the distance between the cations.

B. The mechanism of tunable magnetism

Strain has been widely used to manipulate the actions of electrons and magnetic states of functional materials [48–51]. As we have found, the FM and AFM states in thiospinels correlate closely to the distance between the nearest-neighbor Cr ions. Thus, we have come up with hydrostatic strain as an effective method that can be used to tune the magnetic states in MTM spinel materials. The effects of the strain strength are equivalent to expanding or reducing the distance between Cr ions microscopically. In the equilibrium relaxed structure, MgCr_2O_4 is AFM since $J < 0$, as shown in Fig. 3(c). In fact, MgCr_2O_4 has been regarded as a classical pyrochlore Heisenberg frustrated magnet with Néel temperature (15–20) K [26–28]. In contrast, MgCr_2S_4 and MgCr_2Se_4 are

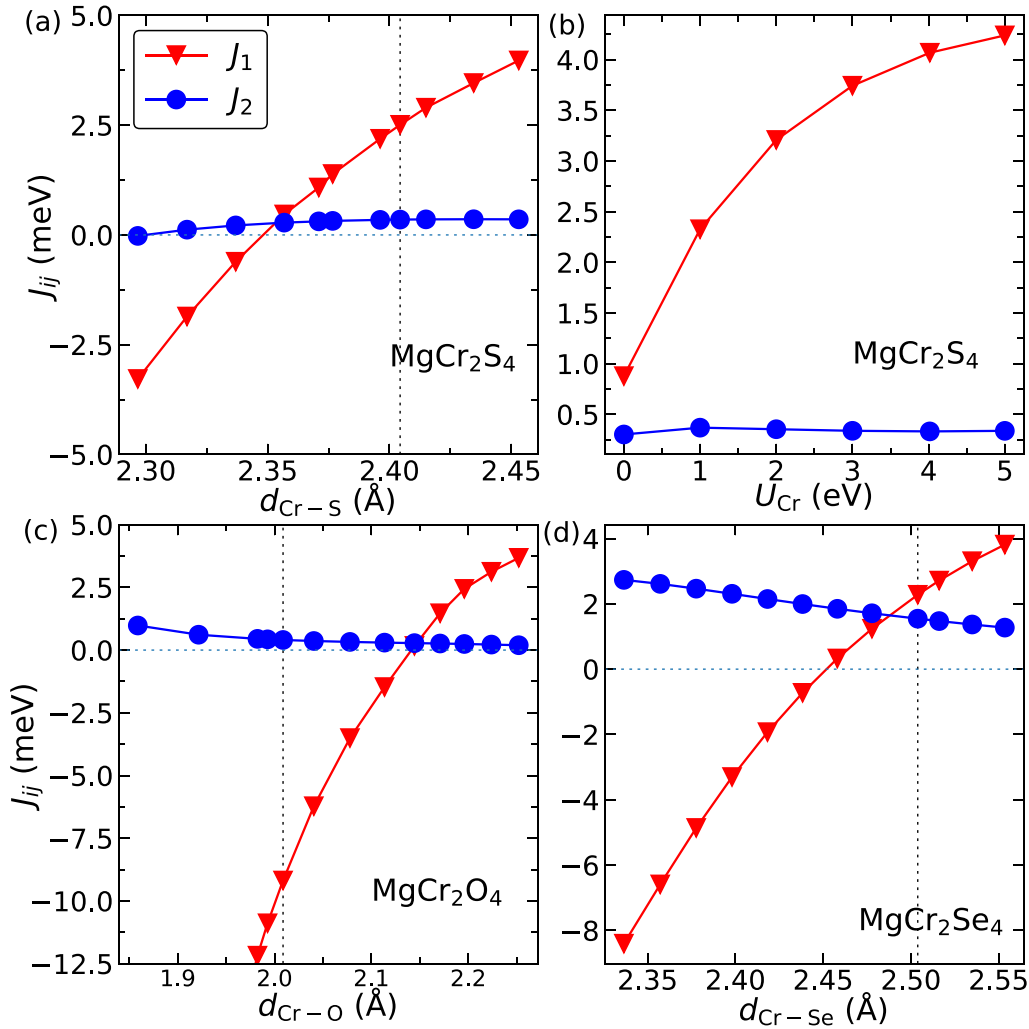


FIG. 3. (a), (c), and (d) The variation of the NN exchange interaction J_1 (red triangles) and the NNN exchange interaction J_2 (blue circles) of $MgCr_2X_4$ ($X = O, S,$ and Se) with the distance between the Cr ions and the anions. The vertical dotted lines represent the equilibrium distances. (b) The computed exchange interactions' variation with the on-site U of $MgCr_2S_4$.

FM at optimal crystal structure, as shown in Figs. 3(a) and 3(d), in which $J > 0$. Figures 3(a), 3(c) and 3(d) show that the Heisenberg exchange coupling coefficients J_1 are extremely sensitive to variation of the distance between the Cr ions and the anions (d_{Cr-X}).

The magnitude of J_1 depends on the strain strength. The variation of J_1 is linear nearly to the bond length. The sign of J_1 even becomes negative when the strong compress strain is used, which indicates the system turns into a frustrated pyrochlore antiferromagnet state. In contrast, the second-order exchange coupling coefficient J_2 retains almost the same value, which illustrates J_2 is nearly independent of the alteration of d_{Cr-X} , as shown in Figs. 3(a), 3(c) and 3(d) by the blue lines with dots. The distance-independent J_2 suggests the overlap between Cr_d and Cr_d is negligible in the second-order d_{Cr-Cr} . Herein, we have shown that the magnetic states of $MgCr_2X_4$ can be FM as well as AFM depending on d_{Cr-X} . Here we are interested in the tensile strain since enhancing J_1 will compensate the demands of applications for strong coupling ferromagnetic (high- T_c) and semiconducting materials.

The origin of the magnetic properties evolving with the distance between the cations can be understood by analyzing the opposite relations between J_{dd} and J_{dpd} . The overall result of exchange interactions, revealed by J_{total} , is decided by the summation of J_{dd} and J_{dpd} . As we described in Sec. IV A, J_{dd} depend on the overlap of t_{2g} orbitals between the two Cr ions. When tensile strain is applied, d_{Cr-Cr} lengthens, and the overlap of t_{2g} orbitals between the two nearest Cr ions shrinks. J_{dd} becomes weak simultaneously. J_{dpd} are little affected by the tiny tensile strain since the hybrid bonding between the e_g orbitals of Cr ions and the p orbitals of anions is very powerful. In other words, these are long-range interactions. The total exchange interactions between the nearest neighbors are their integral contributions.

As a result, J_{dpd} dominates the exchange interactions as the tensile strain is employed. On the other hand, when compress strain is applied, the overlap between the t_{2g} orbitals of Cr ions is substantial. The overall exchange interactions in MTM spinel materials are dominated by J_{dd} , which are antiferromagnetic. Increasing the tensile strain will expand the distance between the two Cr ions, but the t_{2g} orbital

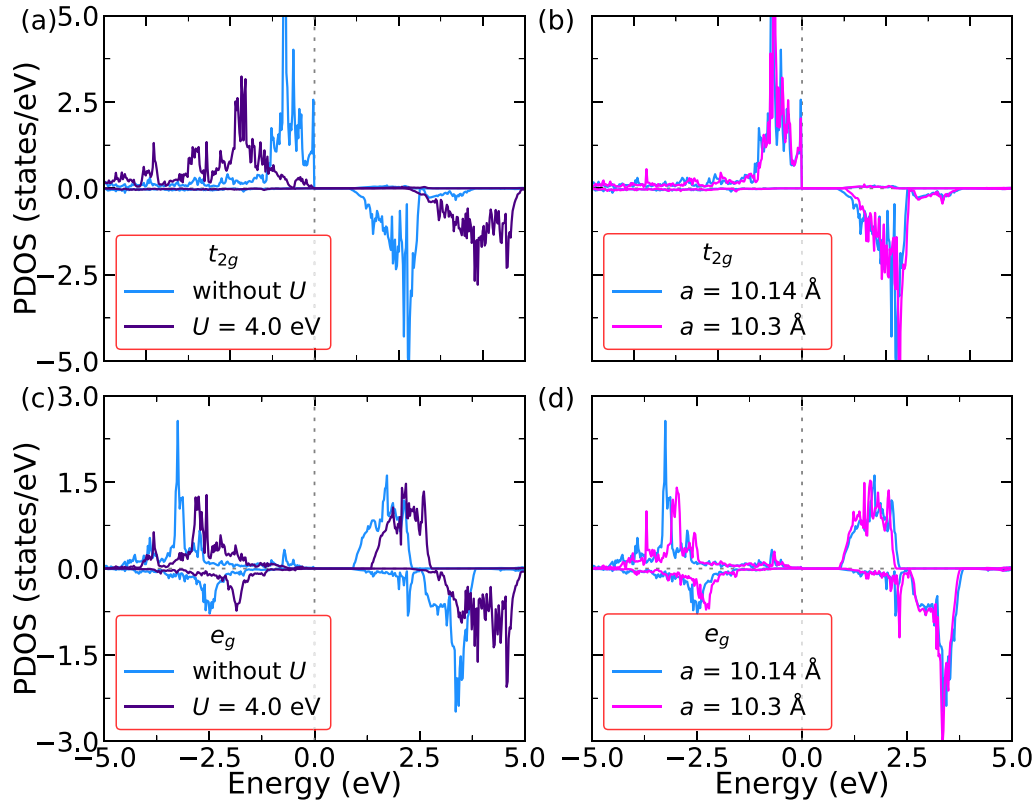


FIG. 4. (a) and (c) The t_{2g} and e_g orbitals' projected density of states (PDOS) of Cr ions of MgCr_2S_4 at different on-site U and lattice constants. The light blue lines show the PDOS in the equilibrium structure without the Hubbard U correction for majority spin and minority spin channels. The indigo lines denote the PDOS from the spin-polarized GGA + U calculation with $U = 4.0$ eV, compared with the results from the $U = 0$ calculation (the light blue curve). (b) and (d) The PDOS at lattice constants $a = 10.14$ Å (optimal structure, light blue curve) and 10.3 Å (tensile strain applied, purple curve), respectively. The Fermi level is set to zero.

character almost remains in the same state whether or not the tensile strain is applied, as shown by the density of states at equilibrium and stretched lattice constants in Figs. 4(b) and 4(d). The localization characters of t_{2g} orbitals are not affected by the tensile strain. The overlap of the two t_{2g} orbitals decreases with the expansion of the distance between the two Cr ions. We will show this phenomenon clearly later.

To verify the robust exchange interactions beyond the GGA approximations involved in the $3d$ transition metals, we also employ the spin-polarized GGA + U method to correct the Cr local $3d$ states. We take only MgCr_2S_4 as an example to inspect the effect of on-site U on the exchange coupling coefficients. The results are shown in Fig. 3(b), which shows that J_1 is always positive for all the tested on-site U values. Moreover, the magnitude of J_1 increases almost linearly with the on-site U . For the second-order exchange, however, J_2 is not affected by the on-site U of Cr, as shown in Fig. 3(b). The exchange splitting of d orbitals between the majority spin and minority spin becomes broad with increasing on-site U values, which is also related to the large band gap, as shown in Figs. 4(a) and 4(c). Furthermore, the t_{2g} orbitals become delocalized when the on-site U is added, and the hybridization between the d orbitals of the Cr ions and the p orbitals of the anions is strengthened in more expansion d orbitals. J_{dpd} will grow stronger as the hybridization between p and d orbitals becomes more intense.

We can understand the variation of J with U by analyzing the d - p - d and the d - d hopping paths. The path that dominates the FM superexchange, as denoted by J_{dpd} , is schematically shown in Fig. 1. This 90° FM superexchange scales as $J_{dpd} \sim \frac{t_{\text{eff}}^2}{2\Delta_{\text{CT}} + U_{pp}} \frac{J_H^p}{2\Delta_{\text{CT}} + U_{pp}}$, where Δ_{CT} is the charge-transfer energy and J_H^p is the Hund's energy of the anions, and the effective d - d hopping is determined by the d - p hopping: $t_{\text{eff}} = t_{dp}^2 / \Delta_{\text{CT}}$. Note that there is no explicit dependence of J_{dpd} on the Hubbard U_{dd} of the transition metal d orbitals. The value of U_{dd} may affect J_{dpd} by indirectly changing the charge-transfer energy Δ_{CT} and/or the d - p hopping t_{dp} . Correspondingly, the enhanced d - p hopping is revealed by the projected DOS (PDOS) in Fig. 4. The more expanded PDOS of the t_{2g} orbitals with $U = 4.0$ eV suggests an increased d - p hopping compared to the hopping without U . Thus, the effective d - d hopping t_{eff} increases as U increases, which results in an increased superexchange J_{dpd} . A more comprehensive description of the magnetic exchange interactions in transition metal compounds can be found in the book by Khomskii [43].

C. A model for the orbital-overlapping integrals

We quantitatively estimate the overlap between two different ion orbitals to demonstrate the change in J_1 with $d_{\text{Cr-Cr}}$. For this purpose, we found that the normal Wannier functions have a disadvantage and they are not a suitable basis to use. In general, the spin magnetic moment that the magnetic

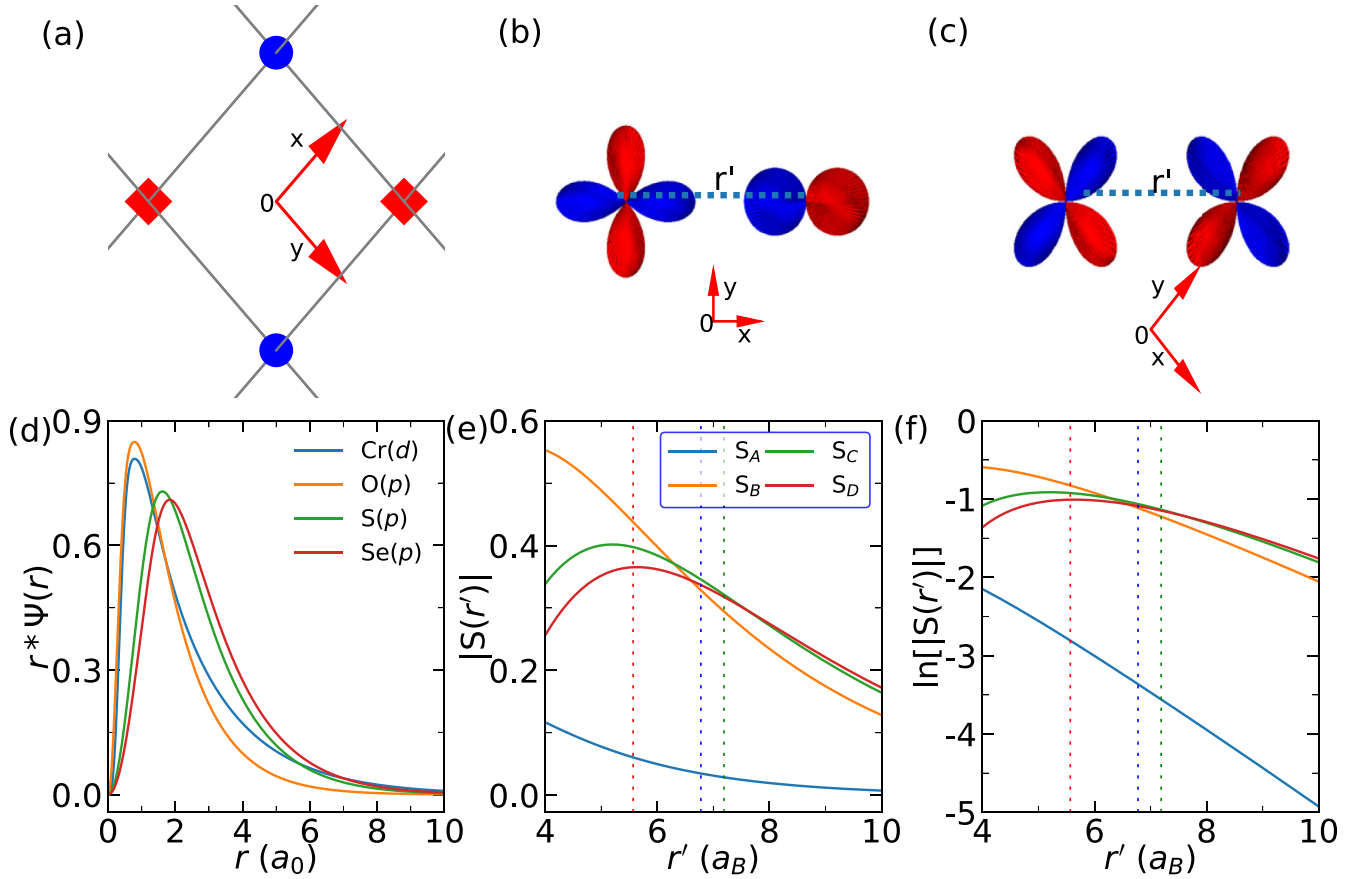


FIG. 5. Distance-dependent orbital overlap $S(r')$ between two ion orbitals. (a) The local crystal structure, where the red squares represent the Cr ions and the blue spheres are X anions ($X = \text{O}, \text{S}, \text{and Se}$). The orbital overlaps depend on the distance r' between the two ions: (b) schematic diagram of the overlap along the x direction between the Cr $d_{x^2-y^2}$ orbital and X p_x orbital and (c) the overlap in the diagonal direction between the Cr d_{xy} orbital and the Cr d_{xy} orbital. (d) The radial part of the valence electrons' pseudo wave functions of the Cr d orbital and the X p orbital. (e) $S(r')$ of two different ion orbitals' pseudo wave functions versus the distance r' between the two ions. $S_A, S_B, S_C,$ and S_D represent the overlaps between different orbitals. (f) The logarithm of the overlap versus the distance r' between the two ions. The vertical dashed lines in (e) and (f) represent r' at DFT optimized structures, MgCr_2O_4 (red), MgCr_2S_4 (blue), and MgCr_2Se_4 (green).

coupling affects is due to the electrons in spin-polarized orbitals. Considering the ligand orbitals are nearly not spin polarized, the wave function corresponding to the spin moment should include no or a small orbital component from the ligand. The Wannier functions are obtained with the initial projection on the Cr d orbitals and ligand p orbitals, in which the non-negligible p -like wave functions at ligands are included in the Wannier orbitals projected on Cr d orbitals. If the Wannier functions are used, the spin magnetic moment will also include orbitals that usually exhibit no spin polarization. On the other hand, there is no preferred basis for calculating J_{dd} and J_{dpl} in general. The key factor is that the magnetic coupling is required to be consistent with the spin magnetic moment obtained from the chosen basis. So we instead employ the ion orbital model in this work. In this model, the overlap integrals between orbitals that approximately represent the relations between the hopping integral and displacement of $r'_{\text{Cr-Cr}}$ and $r'_{\text{Cr-X}}$ are calculated.

We simulated the Cr ions in an octahedral crystal field. The radial part of the ions' pseudo wave functions $R_X(r)$ (where $X = \text{Cr}, \text{O}, \text{S}, \text{and Se}$) was computed with the OPIUM code [52], as shown in Fig. 5(d). The remainder of the ion pseudo wave

functions in the octahedral crystal field was constructed from spherical harmonics [53] Y_{lm} ,

$$d_{x^2-y^2} = \frac{1}{\sqrt{2}} [Y_{2,2}(\vec{r}) + Y_{2,-2}(\vec{r})] = \frac{\sqrt{15}}{4\sqrt{\pi}} \frac{x^2 - y^2}{r^2}, \quad (5)$$

$$d_{xy} = \frac{1}{\sqrt{2}i} [-Y_{2,2}(\vec{r}) + Y_{2,-2}(\vec{r})] = \frac{\sqrt{15}}{2\sqrt{\pi}} \frac{xy}{r^2}, \quad (6)$$

$$p_x = \frac{1}{\sqrt{2}} [Y_{1,-1}(\vec{r}) - Y_{1,1}(\vec{r})] = \frac{\sqrt{3}}{2\sqrt{\pi}} \frac{x}{r}. \quad (7)$$

The ion orbital pseudo wave functions are built by multiplying the two parts. Then the overlap S between two ions is formulated by integrating the ion orbital pseudo wave functions in spherical coordinates, and we define S as

$$S(r') = \iiint \psi(r)\varphi(r-r')r^2 \sin(\theta) dr d\theta d\phi, \quad (8)$$

where $\psi(r) = R_{\text{Cr}}(r) \times d_{x^2-y^2}$ or $\psi(r) = R_{\text{Cr}}(r) \times d_{xy}$ and $\varphi(r-r') = R_X(r-r') \times p_x$ or $\varphi(r-r') = R_{\text{Cr}}(r-r') \times d_{xy}$ (where $X = \text{O}, \text{S}, \text{and Se}$). We calculated four types of overlap to estimate the distance-dependent $S(r')$. $S(r')$

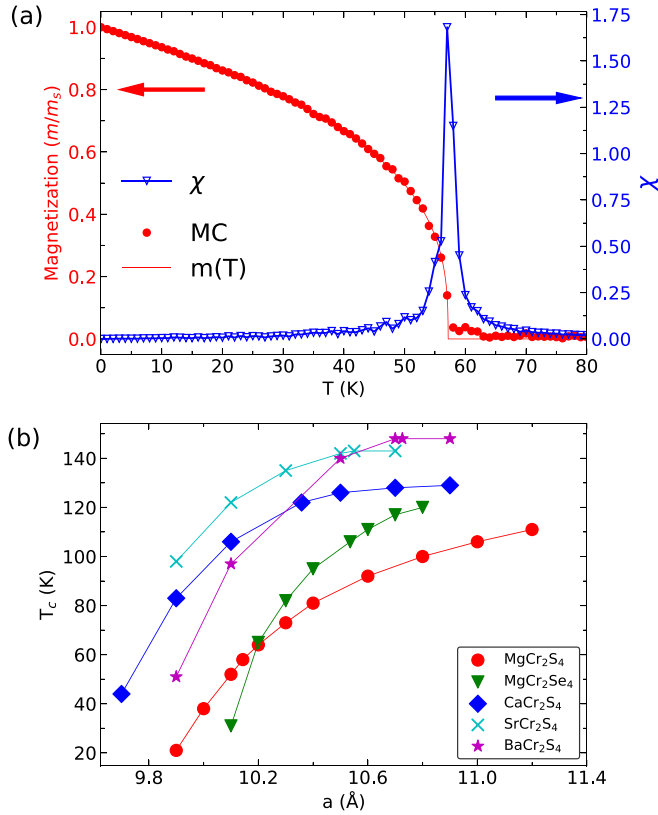


FIG. 6. (a) The normalized magnetization of MgCr_2S_4 (red circles) and susceptibility (blue triangles) versus the temperature simulated with the Monte Carlo (MC) method. The red curve is the temperature-dependent magnetization fit to the Curie-Bloch equation $m(T) = (1 - T/T_c)^\beta$. (b) The variation of the transition temperature T_c with the lattice constant a_0 of the cubic spinel cell predicted by the MC simulation for different MTM spinel materials.

between the Cr ion t_{2g} orbitals in the diagonal direction, as shown in Figs. 5(a) and 5(c), is defined as $S_A(r') = \iiint \psi(r)\varphi(r-r')r^2\sin(\theta)drd\theta d\phi$, where $\psi(r)$, $\varphi(r-r') = R_{\text{Cr}}(r) \times d_{xy}$, $R_{\text{Cr}}(r-r') \times d_{xy}$. The overlap between the Cr ions and the X ($X = \text{O}, \text{S}, \text{and Se}$) ion p orbitals are the same in both the x and y directions, as shown schematically in Figs. 5(a) and 5(b). We define $S_B(r')$, $S_C(r')$, $S_D(r') = \iiint \psi(r)\varphi(r-r')r^2\sin(\theta)drd\theta d\phi$, where $\psi(r) = R_{\text{Cr}}(r) \times d_{x^2-y^2}$ and $\varphi(r-r') = R_X(r-r') \times p_x$ for $X = \text{O}, \text{S}, \text{and Se}$, respectively.

The results for $S_A(r')$, $S_B(r')$, $S_C(r')$, and $S_D(r')$ are shown in Fig. 5(e). There are two points that concern $S(r')$. First, $S(r')$ between $\text{Cr}(d_{xy})$ - $\text{Cr}(d_{xy})$ declines abruptly because the two Cr ions are apart from each other (i.e., r' goes up). It is even close to zero for the equilibration crystal structure, while $S(r')$ for $\text{Cr}(d_{x^2-y^2})$ - $X(p_x)$ are in the range of 0.3–0.4, as shown in Fig. 5(e). Second, the variation of $S_B(r')$, $S_C(r')$, and $S_D(r')$ is remarkably prominent in the zone of press strain ($r'_{\text{Cr-Cr}/X}$ are smaller than that in the equilibration structure), in which $S_B(r')$ is the largest, followed by $S_C(r')$, and $S_D(r')$ is the smallest. However, this order is overturned in the tensile strain zone ($r'_{\text{Cr-Cr}/X}$ are larger than that in the equilibration structure), and $S_{B,C,D}(r')$ varies with r' gradually. The variation of $S(r')$ and its alteration are quite similar to the variance

of the radial part of ion orbital pseudo wave functions [compare Figs. 5(d) and 5(e)].

In general, the degree of locality of the $X(p)$ orbitals is $\text{O} > \text{S} > \text{Se}$. Meanwhile, both $d_{x^2-y^2}$ and p_x orbitals are distributed along the x -axis direction [see Fig. 5(b)], which leads to $S(r')$ aligning in the order $\text{Se} > \text{S} > \text{O}$. The d_{xy} orbital is locally distributed on the x and y axes, in contrast to the diagonal direction, as shown in Fig. 5(c). As a result, $S_A(r')$ drops to zero swiftly with the increase of r' . It is more sensitive to the variation of the distance between the ions. The variation ratios are further revealed by the logarithm of $S(r')$. In Fig. 5(f), the logarithm of $S_A(r')$ shows that $\ln[|S_A(r')|]$ is the steepest of them. The variation with r' of $\ln[|S_B(r')|]$, $\ln[|S_C(r')|]$, and $\ln[|S_D(r')|]$ is similar to $S_B(r')$, $S_C(r')$, and $S_D(r')$, which reduce to zero gently.

These distance-dependent relations for $S_A(r')$, $S_B(r')$, $S_C(r')$, and $S_D(r')$ imply the hoppings t_{dd} and t_{dp} between the ion orbitals depend on $d_{\text{Cr-Cr}/X}$. J_{dd} related to the direct hopping t_{dd} between Cr(d) orbitals can be sustained only in a small range of lattice constants, i.e., short $d_{\text{Cr-Cr}}$, which can be achieved by hydrostatic press strain on the spinel materials. For J_{dp} , however, owing to the lower localization of $X(p)$ and the inline distribution of $\text{Cr}(d_{x^2-y^2})$ and $X(p_x)$ orbitals, the hopping t_{dp} is robust in a wide range of r' and less sensitive to $d_{\text{Cr-X}}$. The considerable and insensitive hopping $t_{p_x-d_{x^2-y^2}}$ indicates the ferromagnetic exchange interactions are strong and can be strengthened indirectly by expanding the distance between the Cr ions with tensile strain. These results conform well to our calculations of the exchange coupling coefficients in thiospinels, as can be seen in Fig. 3. This again verifies that distance-dependent J_{dd} and J_{dp} are controllable in MTM spinel materials.

D. Estimation of transition temperature

With a deep understanding of the ferromagnetic properties and these calculated Heisenberg exchange interaction coefficients, we can use these results to evaluate T_c of AM_2X_4 using the Monte Carlo (MC) method. The classical Heisenberg Hamiltonian $H = \sum_{i<j} J_{ij}\mathbf{S}_i \cdot \mathbf{S}_j$ has been employed to simulate this system, where the magnetic moments \mathbf{S}_i can change their directions but the quantity is fixed. We simulate T_c based on the MC method, which was performed using the VAMPIRE software package [54].

The MC simulations use 50 000 equilibrations and averaging steps. We consider a system in the simple cubic cell with 16 Cr atoms with nearest- and near-nearest-neighbor exchange included. The periodic boundary condition was used, along with a supercell size of $20 \times 20 \times 20 \text{ nm}^3$, including 128 000 Cr atoms, which is large enough to lead to the convergence of T_c after different supercells are used in the convergence test. The results of these calculations are shown in Fig. 6(a), where the magnetization was normalized. From the normalized magnetization and the magnetic susceptibility χ versus temperature, we can extract the transition temperature, which is 57 K in this case. The magnetization at T_c has a tail because of the finite size supercell considered here. It is hard to estimate the transition temperature from the original MC normalized magnetic moments due to the tail. In the

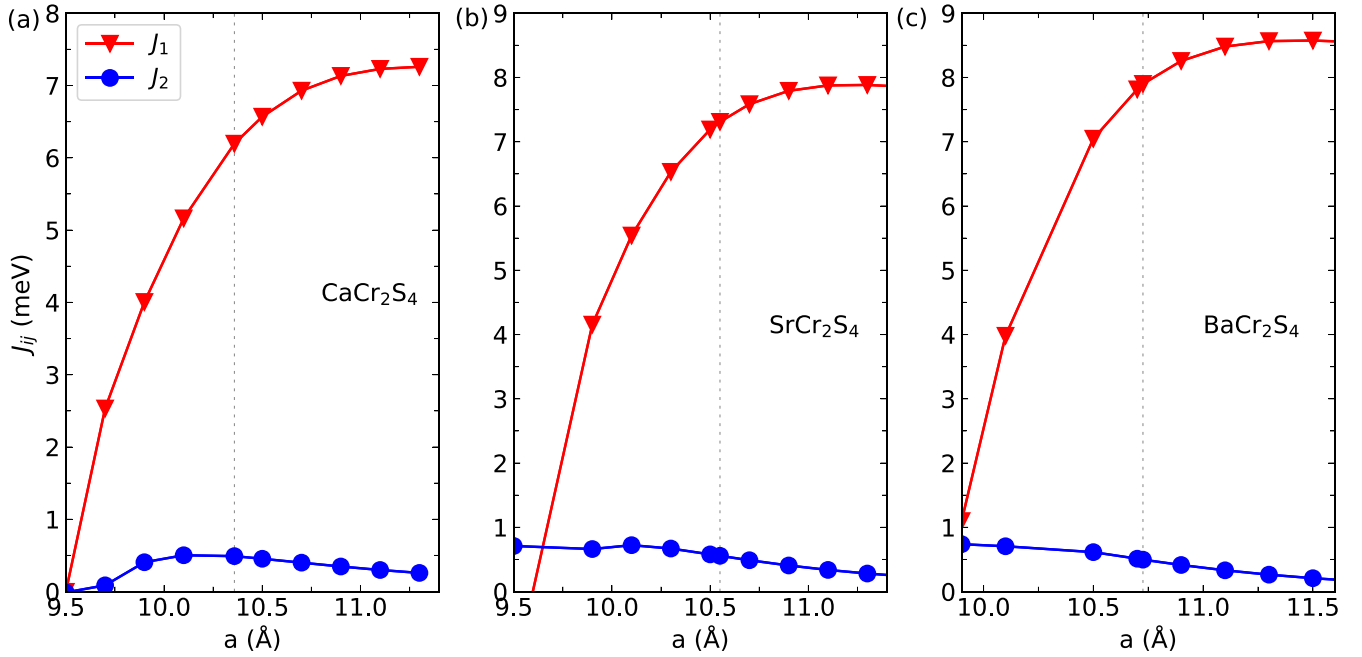


FIG. 7. The NN exchange interaction coefficients J_1 (red triangles) and the NNN exchange interaction J_2 (blue circles) of ACr_2S_4 ($A = Ca, Sr, Ba$) variation with the lattice constants. The vertical dashed line represents the lattice constants of the optimized structure.

susceptibility, however, there is a sharp peak at T_c . We can determine T_c according to the peak position of $\chi(T)$.

The temperature-dependent magnetization can be fitted with the Curie-Bloch equation in the classical limit [55]:

$$m(T) = \left(1 - \frac{T}{T_c}\right)^\beta, \quad (9)$$

where T represents temperature, T_c is the Curie temperature, and β is the critical exponent. The results of the fitting are shown by the red curve in Fig. 6(a), which matches the MC simulation results. From the classical fitting curve, we determine T_c is 57 K, which is equal to the result derived from the temperature-dependent susceptibility, and the exponent β is 0.338 by fitting. Figure 6(b) indicates the T_c increase with the unit cell expansion. T_c depends on the exchange interactions directly, while the exchange interactions correlate to d_{Cr-Cr} between the ions and the on-site U of Cr ions. As a consequence, T_c is affected indirectly by both of them.

The ferromagnetism becomes remarkable in $MgCr_2Se_4$ and $MgCr_2S_4$ as we increase d_{Cr-Cr} , as shown in Fig. 3. We conjecture that substituting A site ions with larger ions (such as Ca, Sr, and Ba) to construct different MTM spinel materials will result in higher T_c . The exchange coupling coefficients of ACr_2S_4 ($A = Ca, Sr, Ba$) are summarized in Fig. 7. Like for $MgCr_2S_4$, J_1 increases linearly with the lattice constants. On the contrary, J_2 changes slightly with the lattice constant. The magnetic states are FM for ACr_2S_4 ($A = Ca, Sr, Ba$) in a large range around the equilibrant structure. Our MC simulation results for T_c are shown in Fig. 6(b), which demonstrates the alternative alkaline metals in MTM spinel materials have higher T_c than that in $MgCr_2S_4$. These T_c are also strain dependent, which is in agreement with our proposal to envisage

a scheme to implement high T_c with tensile strain in MTM spinel materials.

V. CONCLUSION

In conclusion, we uncovered the magnetic coupling mechanism of the FM and AFM states in thiospinels, where, as a special example of the named MTM spinel materials, $MgCr_2X_4$ ($X = O, S, Se$) and ACr_2S_4 ($A = Ca, Sr, Ba$) were used to explore the tunable properties of magnetism and electronic structures. We verified that the magnetic states in thiospinels can change between FM and AFM. Therefore, the magnetic structures of the MTM spinel material can be tuned by ion substitution and the strain method. The ferromagnetic properties are strengthened with tensile strain, as J_{dd} between the cations becomes negligible.

Based on MC simulations, we predicted T_c of FM states, and T_c is considerable when tensile strain is applied. Currently, only $MgCr_2S_4$ has been synthesized in the experiment, and T_c is too low for practical application. Our study results suggest that T_c can be improved by tensile strain or the ion substitution approach or both. Our results will expand the applicability of spinel materials for applications in spintronic devices because T_c are tunable by external strain and ion substitution. In addition, the transition of the magnetic states between FM and AFM will trigger the study of magnetic mechanisms in MTM spinel materials. Especially, the AFM state, which is the classical pyrochlore Heisenberg frustrated magnet system, will lead to additional discovery of classical spin liquids, spin glass states, frustrated magnetism, etc.

ACKNOWLEDGMENTS

This work was supported by the National Key R&D Program of China (Grant No. 2022YFA1402401) and the

National Natural Science Foundation of China (Grant No. 11521404). Computational resources were supported by the

Center for High Performance Computing at Shanghai Jiao Tong University.

-
- [1] T. Dietl, *Acta Phys. Pol. A* **100**, 139 (2001).
- [2] H. Ohno, *J. Magn. Magn. Mater.* **242**, 105 (2002).
- [3] S. A. Wolf, *Science* **294**, 1488 (2001).
- [4] K. Ando, *Science* **312**, 1883 (2006).
- [5] B. T. Matthias, R. M. Bozorth, and J. H. Van Vleck, *Phys. Rev. Lett.* **7**, 160 (1961).
- [6] P. K. Baltzer, H. W. Lehmann, and M. Robbins, *Phys. Rev. Lett.* **15**, 493 (1965).
- [7] M. A. Subramanian, A. P. Ramirez, and W. J. Marshall, *Phys. Rev. Lett.* **82**, 1558 (1999).
- [8] H. Das, U. V. Waghmare, T. Saha-Dasgupta, and D. D. Sarma, *Phys. Rev. Lett.* **100**, 186402 (2008).
- [9] Y. K. Wakabayashi, Y. Krockenberger, N. Tsujimoto, T. Boykin, S. Tsuneyuki, Y. Taniyasu, and H. Yamamoto, *Nat. Commun.* **10**, 535 (2019).
- [10] S. Das, A. Halder, A. Chakraborty, I. Dasgupta, and T. Saha-Dasgupta, *Phys. Rev. B* **101**, 184422 (2020).
- [11] G. D. Rieck and J. J. M. Thijssen, *Acta Crystallogr., Sect. B* **24**, 982 (1968).
- [12] Y. H. Hou, Y. J. Zhao, Z. W. Liu, H. Y. Yu, X. C. Zhong, W. Q. Qiu, D. C. Zeng, and L. S. Wen, *J. Phys. D* **43**, 445003 (2010).
- [13] T. Yamanaka and Y. Takéuchi, *Z. Kristallogr.* **165**, 65 (1983).
- [14] T. Masuda, A. Zheludev, A. Bush, M. Markina, and A. Vasiliev, *Phys. Rev. Lett.* **92**, 177201 (2004).
- [15] M. Coey, *Nature (London)* **430**, 155 (2004).
- [16] M. S. Senn, J. P. Wright, and J. P. Attfield, *Nature (London)* **481**, 173 (2012).
- [17] E. Verwey and P. Haayman, *Physica (Amsterdam)* **8**, 979 (1941).
- [18] A. Kumar, C. J. Fennie, and K. M. Rabe, *Phys. Rev. B* **86**, 184429 (2012).
- [19] J. P. Wright, J. P. Attfield, and P. G. Radaelli, *Phys. Rev. Lett.* **87**, 266401 (2001).
- [20] T. Suzuki, M. Katsumura, K. Taniguchi, T. Arima, and T. Katsufuji, *Phys. Rev. Lett.* **98**, 127203 (2007).
- [21] V. O. Garlea, R. Jin, D. Mandrus, B. Roessli, Q. Huang, M. Miller, A. J. Schultz, and S. E. Nagler, *Phys. Rev. Lett.* **100**, 066404 (2008).
- [22] Y. Tokura, *Science* **288**, 462 (2000).
- [23] Q. Mahmood, N. Noor, M. Jadan, J. S. Addasi, A. Mahmood, and S. M. Ramay, *J. Solid State Chem.* **285**, 121261 (2020).
- [24] A. Miura, H. Ito, C. J. Bartel, W. Sun, N. C. Rosero-Navarro, K. Tadanaga, H. Nakata, K. Maeda, and G. Ceder, *Mater. Horiz.* **7**, 1310 (2020).
- [25] A. Wustrow, B. Key, P. J. Phillips, N. Sa, A. S. Lipton, R. F. Klie, J. T. Vaughey, and K. R. Poeppelmeier, *Inorg. Chem.* **57**, 8634 (2018).
- [26] S. E. Dutton, Q. Huang, O. Tchernyshyov, C. L. Broholm, and R. J. Cava, *Phys. Rev. B* **83**, 064407 (2011).
- [27] H. Ehrenberg, M. Knapp, C. Baetz, and S. Klemme, *Powder Diffr.* **17**, 230 (2002).
- [28] K. W. Plumb, H. J. Changlani, A. Scheie, S. Zhang, J. W. Krizan, J. A. Rodriguez-Rivera, Y. Qiu, B. Winn, R. J. Cava, and C. L. Broholm, *Nat. Phys.* **15**, 54 (2019).
- [29] X. Zhang, V. Stevanović, M. d’Avezac, S. Lany, and A. Zunger, *Phys. Rev. B* **86**, 014109 (2012).
- [30] P. Hohenberg and W. Kohn, *Phys. Rev.* **136**, B864 (1964).
- [31] W. Kohn and L. J. Sham, *Phys. Rev.* **140**, A1133 (1965).
- [32] G. Kresse and J. Furthmüller, *Phys. Rev. B* **54**, 11169 (1996).
- [33] G. Kresse and J. Furthmüller, *Comput. Mater. Sci.* **6**, 15 (1996).
- [34] G. Kresse and D. Joubert, *Phys. Rev. B* **59**, 1758 (1999).
- [35] P. E. Blöchl, *Phys. Rev. B* **50**, 17953 (1994).
- [36] J. P. Perdew, K. Burke, and M. Ernzerhof, *Phys. Rev. Lett.* **77**, 3865 (1996).
- [37] H. J. Monkhorst and J. D. Pack, *Phys. Rev. B* **13**, 5188 (1976).
- [38] A. Togo and I. Tanaka, *Scr. Mater.* **108**, 1 (2015).
- [39] X. Gonze and C. Lee, *Phys. Rev. B* **55**, 10355 (1997).
- [40] S. Baroni, S. de Gironcoli, A. Dal Corso, and P. Giannozzi, *Rev. Mod. Phys.* **73**, 515 (2001).
- [41] S. L. Dudarev, G. A. Botton, S. Y. Savrasov, C. J. Humphreys, and A. P. Sutton, *Phys. Rev. B* **57**, 1505 (1998).
- [42] C. Kant, J. Deisenhofer, V. Tsurkan, and A. Loidl, *J. Phys.: Conf. Ser.* **200**, 032032 (2010).
- [43] D. I. Khomskii, *Transition Metal Compounds* (Cambridge University Press, Cambridge, 2014).
- [44] J. Kanamori, *J. Phys. Chem. Solids* **10**, 87 (1959).
- [45] P. W. Anderson, *Phys. Rev.* **115**, 2 (1959).
- [46] J. B. Goodenough, *Phys. Rev.* **100**, 564 (1955).
- [47] X. Bai, J. A. M. Paddison, E. Kapit, S. M. Koohpayeh, J. J. Wen, S. E. Dutton, A. T. Savici, A. I. Kolesnikov, G. E. Granroth, C. L. Broholm, J. T. Chalker, and M. Mourgial, *Phys. Rev. Lett.* **122**, 097201 (2019).
- [48] C. Peng, Y. Wang, Z. Cheng, G. Zhang, C. Wang, and G. Yang, *Phys. Chem. Chem. Phys.* **17**, 16536 (2015).
- [49] B. L. Chittari, D. Lee, N. Banerjee, A. H. MacDonald, E. Hwang, and J. Jung, *Phys. Rev. B* **101**, 085415 (2020).
- [50] M. Zhang, X. Wang, X. Wang, Y. Wang, M. Wei, and M.-Y. Ni, *Mod. Phys. Lett. B* **33**, 1950304 (2019).
- [51] D. Meng, H. Guo, Z. Cui, C. Ma, J. Zhao, J. Lu, H. Xu, Z. Wang, X. Hu, Z. Fu, R. Peng, J. Guo, X. Zhai, G. J. Brown, R. Knize, and Y. Lu, *Proc. Natl. Acad. Sci. USA* **115**, 2873 (2018).
- [52] OPIUM, <http://opium.sourceforge.net>.
- [53] H. Tai, *Phys. Rev. A* **45**, 1454 (1992).
- [54] R. F. L. Evans, W. J. Fan, P. Chureemart, T. A. Ostler, M. O. A. Ellis, and R. W. Chantrell, *J. Phys.: Condens. Matter* **26**, 103202 (2014).
- [55] N. W. Ashcroft and N. D. Mermin, *Solid State Physics* (Holt, Rinehart and Winston, New York, 1976).